BATCH: nl2a14 USER: jeh69 DIV: @xyv04/data1/CLS_pj/GRP_nl/JOB_i02/DIV_nl0481829 DATE: January 3, 20

NANO LETTERS

xxxx
Vol. 0, No. 0
A−F

Deflection of Nanotubes in Response to External Atomic Collisions

Ki-Ho Lee,† Pawel Keblinski,‡ and Susan B. Sinnott*

Department of Materials Science and Engineering, University of Florida, Gainesville, Florida 32611-6400, and Materials Science and Engineering Department, Rensselaer Polytechnic Institute, Troy, New York, 12180-3590

Received November 2, 2004; Revised Manuscript Received December 16, 2004

ABSTRACT

The mechanical response of single-walled and multiwalled carbon nanotubes to a series of external Ar atom impacts is examined with classical molecular dynamics simulations. The extent to which the carbon nanotubes deform in the direction perpendicular to their axis is found to depend on the amount of momentum transferred during the collisions. The details of the mechanical response and recovery of the nanotubes after release are also found to depend on the nanotube configurations.

The electrical and mechanical properties of carbon nanotubes have extended the potential applications of nanoelectromechanical systems (NEMS) such as nanoswitches,[1] nanosensors,[2] nanoactuators,[3] and nanotweezers.[4] Such devices are based on inducing external forces through the application of electric currents that flow through the nanotubes. In these cases, the force field is continuously varied over the entire material. When the nanotubes are exposed to irregular force fields, such as those induced by an irregular gas flow, the behavior will be different from the behavior of the nanotube under constant electrostatic fields. Irregularities in geometry or time can cause local heating, deformation, and damage. There is, therefore, incentive to investigate the mechanical responses of nanotubes to a variety of external stimuli.

Despite the experimental difficulties inherent in measuring the mechanical properties of nanotube samples, the moduli and strengths of nanotubes have been obtained from various experiments, such as radial compression, tensile-loading, and bending tests using atomic force microscopy and transmission electron microscopy.[5−9] Similarly, insight into load transfer mechanisms[10] and strain energy effects[11−13] has been achieved using computational methods. Furthermore, computational methods have investigated the mechanics of complex structures of gas-filled nanotubes,[14] deformation of nanotubes through torsion,[15,16] and elastic and plastic deformations under tensile loads.[17−19]

In addition, the dynamics of nanotube mechanics has been studied computationally with molecular dynamics (MD) simulations to evaluate nanotubes for use in applications such as nanooscillators[20,21] and nanobearings[22,23] which might take advantage of the low friction between the walls of multiwalled nanotubes (MWNTs). The translational oscillation of inner nanotubes in the direction of the nanotube axis has been estimated to be as fast as 1 GHz.[20] The phonon energy is dissipated via a wavy deformation in the outer nanotube vibrating in the radial direction. Transverse vibration of single-walled nanotubes (SWNTs) by thermal energy is also predicted.[24] The amplitudes of the transverse vibration proportionally increase with temperature, whereas the frequencies are constant. This result was obtained, however, with a model where harmonic springs were used to describe C−C bond. With Brenner or Tersoff potentials, the C−C bonds soften with increasing temperature because of anharmonicity. Furthermore, the tube diameter is almost temperature independent. This will lead to a decrease of bending mode frequencies with increasing temperature.[25]

When nanotubes are exposed to an externally flowing fluid, the whole nanotube can be bent, translated, and buckled. Understanding the mechanical response of the nanotube subjected to a gas flow is important for NEMS-device-related applications, such as nanovalves, which control the flow rate of fluid through nanometer-scale channels. In this work we examine the response of single and multiwalled nanotubes to impacts with noble gas atoms using classical MD simulations to predict the motion of nanotubes when they are used for the devices located in the path of pulsed fluid flow.

In the simulations, Newton's equations of motions are numerically integrated with a third-order Nordsieck predictor-corrector integration algorithm to track the motion of the atoms with time. The time step used for the integration is 0.2 fs in all the simulations. The forces on the atoms are calculated using methods that vary with distance: short-range

* Corresponding author. E-mail: ssinn@mse.ufl.edu.
† University of Florida.
‡ Rensselaer Polytechnic Institute.

10.1021/nl0481829 CCC: $30.25 © xxxx American Chemical Society
Published on Web 00/00/0000

PAGE EST: 5.6

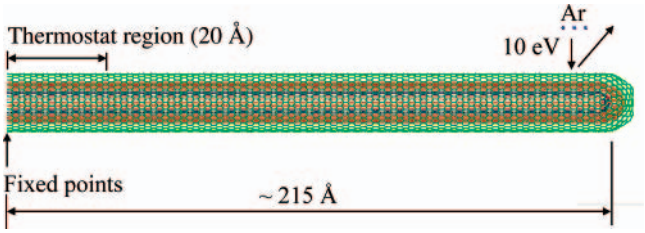

Figure 1. Schematic illustration of Ar collisions on a representative nanotube consisting of a zigzag (10,0)@(19,0)@(28,0) MWNT.

Table 1. Diameters and Number of Atoms of Individual 215 Å Long SWNTs Considered

tube type	dia. (Å)	number of atoms	tube type	dia. (Å)	number of atoms
(10,0)	7.94	2010	(6,6)	8.25	2100
(19,0)	15.08	3906	(11,11)	15.13	3926
(28,0)	22.23	5846	(16,16)	22.00	5820

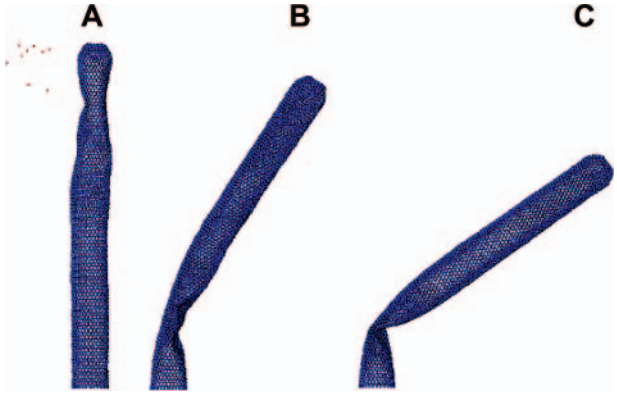

Figure 2. Snapshots of a (28,0) SWNT after a series of Ar atom collisions and during subsequent relaxation. (A) The nanotube after the first collision event. (B) The nanotube after the tenth collision event. (C) The nanotube after relaxing for 40 ps. The left-most end was held rigid throughout as described in the text.

interactions are calculated using the second generation of Brenner's reactive, empirical bonding-order (REBO) hydrocarbon potential[26] that realistically describes covalent bonding within carbon nanotubes. The long-range interactions between nonbonded atoms such as argon and carbon are characterized with a Lennard-Jones (LJ) potential.

The nanotubes considered are SWNTs and two kinds of MWNTs: double-walled nanotubes (DWNTs), and triple-walled nanotubes (TWNT). In particular, the SWNT is either a (28,0) or (16,16) nanotube, the DWNT consists of a (19,0)@(28,0) or (11,11)@(16,16) configuration, and the TWNT consists of a (10,0)@(19,0)@(28,0) or (6,6)@(11,11)@(16,16).[1] These diameters were chosen so that the interlayer spacings would be about 3.4−3.6 Å, in agreement with experimental data.[28,29] The diameters of all the nanotubes used are shown in Table 1. (The notation (19,0)@(28,0) denotes that the MWNT consists of an inner (19,0) nanotube and an outer (28,0) nanotube.[27])

The nanotubes are open at one end and capped at the other. The open ends are firmly fixed in space to mimic the attachment of the nanotubes to a rigid surface. Langevin thermostats are applied to the atoms that are within 20 Å of the open end to dissipate any excess heat transferred to the nanotubes through the collisions and thus maintain a temperature of 300 K. This mimics the transfer of thermal energy from the nanotube to the rigid surface to which it is attached. The length of the nanotubes is about 215 Å excluding the hemispherical caps. All the bonds that connect the nanotubes and caps are sp^2-hybridized, and all defects at the cap−nanotube interface consist of pentagon and heptagon rings. Figure 1 shows a schematic of the system setup, and Table 1 provides information about the total number of atoms in each nanotube.

The gas flow is mimicked by a sequence of collisions events. For each collision event nine Ar atoms impact the nanotube. Each collision event of nine atoms impacting the nanotube is completed in about 2 ps. Up to 10 events are considered here, where nine Ar atoms collide with the nonrigid, capped nanotube end in each event. These Ar atoms are initially located in an 8 Å × 8 Å square 200 Å from the fixed points at the end of the nanotube, and 20 Å above the uppermost atoms of the outer nanotube wall in each system. All nine atoms are then assigned with a kinetic energy of 10 eV/atom, which corresponds to a velocity of 0.0694 Å/fs (6.94×10^3 m/s). This kinetic energy was empirically chosen so as to transfer significant amounts of energy to the nanotubes without damaging their structure and as a computationally efficient way of modeling the transfer of kinetic energy from many more fluid particles moving at slower rates to the nanotubes. After each series of collision events, the nanotubes are relaxed for 100−140 ps.

Figure 2A shows a typical snapshot after the first Ar collision event onto the (28,0) SWNT. The nanotube hardly moves after this first collision event; rather, only the tip of the nanotube deforms, and then the energy from the collision is transferred along the nanotube length, as illustrated in Figure 2A. This behavior is also seen for the MWNTs, but the extent of deformation is much less than in the case of the SWNTs because of the increased nanotube stiffness caused by the presence of multiple nanotube walls in the structure.[30]

After 10 collision events, the nanotube bends and "rumples" form in the wall structure, as shown in Figure 2B. The number of the rumples and their size are related to the extent of deflection. For example, the rumples that form in the DWNTs and TWNTs are much smaller than in the case of the SWNTs. In addition, after 10 collision events, the nanotubes are bent and remain so for some time as the system relaxes. The SWNT, which is more flexible than the DWNTs and TWNTs, even buckles over during relaxation, as shown in Figure 2C. On the whole, the surface of the SWNT during relaxation is much smoother than it is during the actual collision events (compare Figure 2C to Figure 2A). This nanotube buckling is predicted to occur only in the SWNT system and is eventually removed when the SWNT recovers its original shape and structure without plastic deformation or any bond breakage. According to this result it is found that SWNTs have both considerable flexibility and resilience in the direction normal to their axes. The DWNTs and

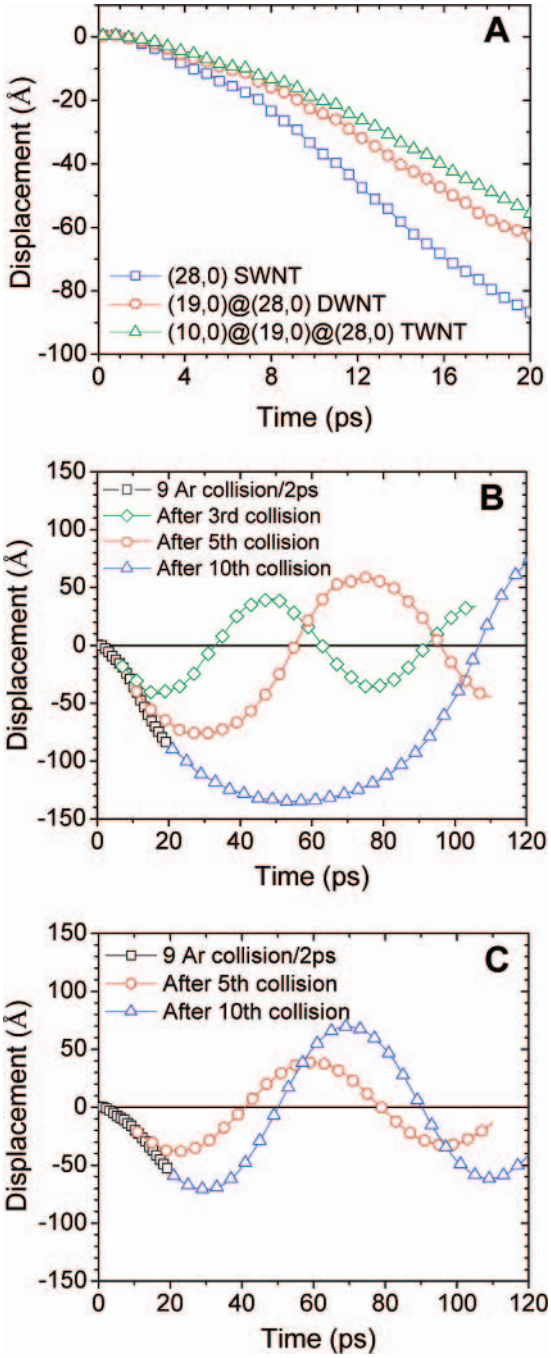

Figure 3. (A) Comparison of the displacements of a SWNT, DWNT, and TWNT after the same number of collision events (up to 10) with Ar. (B) The displacement of a (28,0) SWNT, and (C) the displacement of a (10,0)@(19,0)@(28,0) TWNT after collision events with Ar and relaxation.

TWNTs deform to a much smaller degree than do the SWNTs because of the added stiffness of the additional nanotube shells.

After the first collision event, only the appearance of the nanotube surface is changed and there is no net displacement of the nanotube tip for all the nanotubes considered here. However, as the collision events continue, all the nanotubes move in the direction of Ar flow. Figure 3 shows how the nanotube tips are displaced over time. The displacement of the nanotube is calculated by averaging the displacements

Table 2. Characterization of Nanotube Oscillation for Various Zigzag, 215 Å Long Carbon Nanotubes

	A_0 (Å)	φ (rad)	τ (ps)	f (GHz)	Q
After 5 Collision Events					
SWNT	86.2	1.499	167	11.36	11.9
DWNT	44.9	1.125	553	14.93	51.9
TWNT	39.3	1.005	479	13.33	40.1
After 10 Collision Events					
SWNT	150.1	1.257	324	5.88	12.0
DWNT	88.4	1.086	175	12.35	13.6
TWNT	71.7	0.707	576	12.50	45.2

of the same three carbon atoms located 215 Å from the fixed end. The results indicate that the SWNTs displace more easily than the DWNTs and TWNTs after repeated collision events. This is not surprising because the larger number of nanotube walls raise the mass and thus the inertia of the carbon nanotubes. Furthermore, for a larger number of collision events the SWNTs buckle, which dramatically decreases their bending stiffness and leads to both large amplitude bending and relatively large period of oscillatory motion. As shown in Figure 3C, increasing the number of collision events increases the amplitude of the oscillations as the momentum transferred to the system is larger.

Since the nanotubes flex in an oscillatory manner, the motion of the nanotubes during the relaxation period can be described in terms of amplitude and frequency as follows:

$$A = -A_0 \cos(2\pi ft - \varphi)e^{-t/\tau} \quad (1)$$

where A_0 is the estimated amplitude at the initial state of the relaxation process, f is frequency, t is time in ps, φ is angular phase shift, and τ is relaxation time. A_0 is greater than the initial downward displacement if the oscillation of a nanotube is delayed by φ. The parameters in eq 1 for various zigzag, 215 Å-long nanotubes are shown in Table 2. The quality factor Q ($= 2\pi f\tau$) is also calculated to compare the extent of damping for various cases.

According to Table 2, the frequencies of SWNT oscillation are the smallest predicted in this study, and the frequencies of DWNT oscillation are the largest predicted. This, at first sight, might be surprising considering that the continuum-level formula for the frequency of a tube clamped at one end is[8]

$$f = \frac{0.2798}{L^2}\sqrt{\frac{Y(a^2 + b^2)}{\rho}} \quad (2)$$

where L is the tube length, Y is its Young's modulus, a and b are the inner and outer diameters, respectively, and ρ is the density. Since for all tubes considered the outer diameter is the same, the highest frequency should characterize the SWNT. However, the formula above is only applicable to tubes that bend, and it breaks down when buckling occurs. Consequently, the frequencies associated with SWNT deformation in this study are significantly lower than those

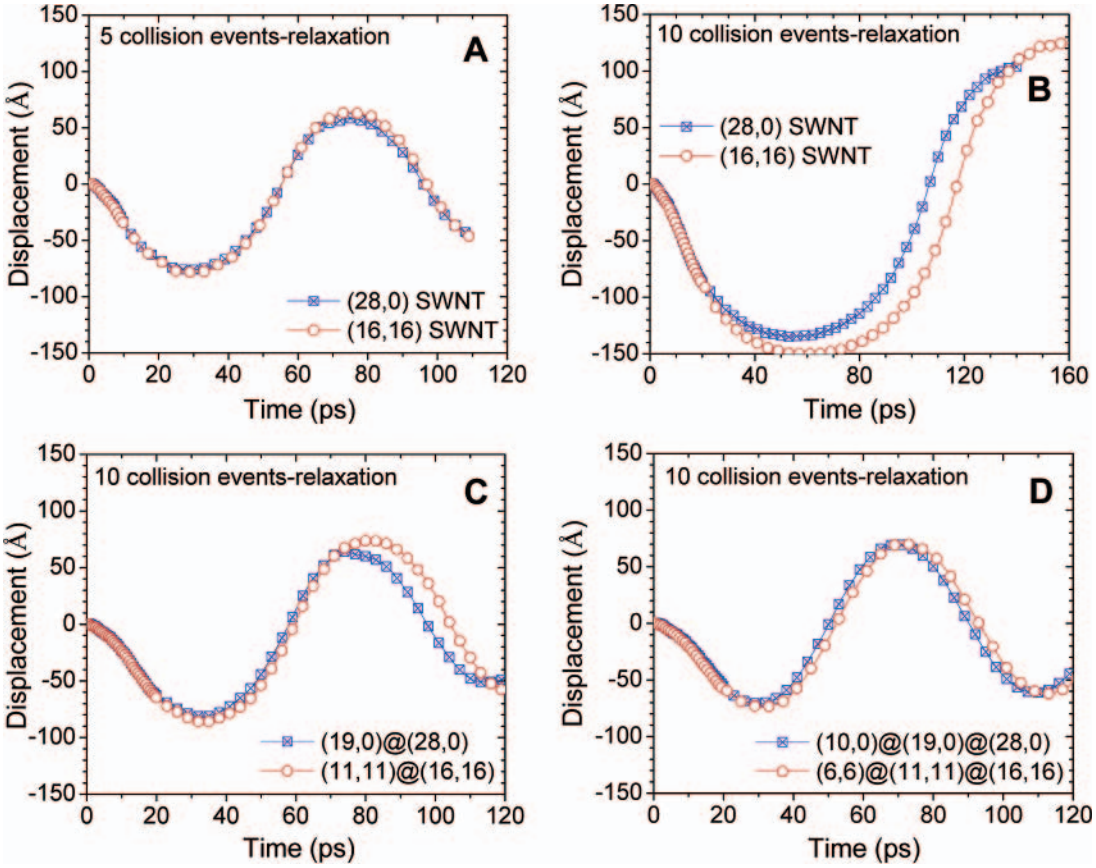

Figure 4. Relative displacements of armchair and zigzag nanotubes after multiple collision events with Ar. (A) Five collision events followed by relaxation and (B) ten collision events followed by relaxation of (28,0) and (16,16) SWNTs. (C) Ten collision events followed by relaxation of (19,0)@(28,0), and (10,10)@(16,16) DWNTs. (D) Ten collision events followed by relaxation of (10,0)@ (19,0)@(28,0), and C) (10,0)@ (11,11)@(16,16) TWNTs.

predicted from eq 2. Buckled nanotubes are also characterized by very large damping of oscillations, i.e., low quality factor, Q, which has its origin in the highly nonlinear behavior at large C−C bond strains in the buckled region. The low Q for the DWNT after 10 collisions (13.6 in Table 2) is also caused by buckling of its outer wall.

The displacements of several armchair nanotubes are compared with the displacements of several zigzag nanotubes in Figure 4. Figure 4A shows coincidence of the displacements for five collision events followed by relaxation in the case of the (28,0) and (16,16) SWNTs. However, more sluggish responses are predicted to occur for the (16,16) SWNTs and the (11,11)@(16,16) DWNTs after 10 collision events and relaxation than in the case of the zigzag nanotubes, as shown in Figure 4B and 4C. Table 3 shows the parameters for eq 1 for armchair nanotubes in order to compare the differences between the displacements of the zigzag and armchair nanotubes that appear when the nanotubes are buckled.

It has been reported[11] that the strain energy of nanotubes depends not on their chiralities but on their radii. It has also been predicted that some mechanical properties of nanotubes, such as the Young's modulus, bending stiffness, and torsion stiffness, depend only on the radius.[31] Therefore, the identical responses to Ar collisions shown in Figures 4A and 4D for different types of chiralities agree with some reported results.

Table 3. Characterization of Nanotube Oscillation for Various Armchair, 215 Å Long Carbon Nanotubes

	A_0 (Å)	φ (rad)	τ (ps)	f (GHz)	Q
After 5 Collision Events					
SWNT	85.4	1.300	226	10.87	15.4
DWNT	47.8	1.077	447	14.29	40.1
TWNT	43.7	1.061	441	12.98	36.0
After 10 Collision Events					
SWNT	161.8	1.269	536	5.05	17.0
DWNT	90.5	0.936	297	10.64	19.9
TWNT	74.9	0.766	484	12.20	37.1

However, according to the work of Yakobson and co-workers and Zhang et al.,[13,32] the yield strength for the plastic deformation depends on nanotube chirality. Thus, the discrepancy between the displacements of zigzag and armchair nanotubes in Figures 4B and 4C may be caused by the differing energetics of the highly deformed sections of the nanotubes. Figure 5 shows the difference of potential energies of zigzag (28,0) and armchair (16,16) nanotubes during deflection. Before the Ar collision events, the potential energy of the (28,0) SWNT is lower than that of the (16,16) by 4.38×10^{-3} eV/atom. Additionally, the armchair (16,16) SWNT has lower potential energy than the zigzag (28,0) SWNT, even when the (16,16) SWNT is deformed to a larger

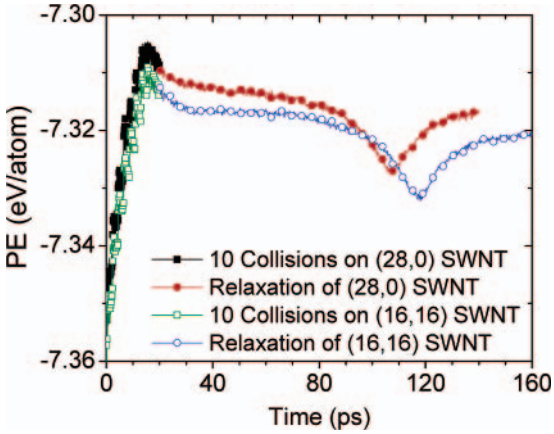

Figure 5. Potential energy variation of zigzag (28,0) and armchair (16,16) SWNTs during deflection.

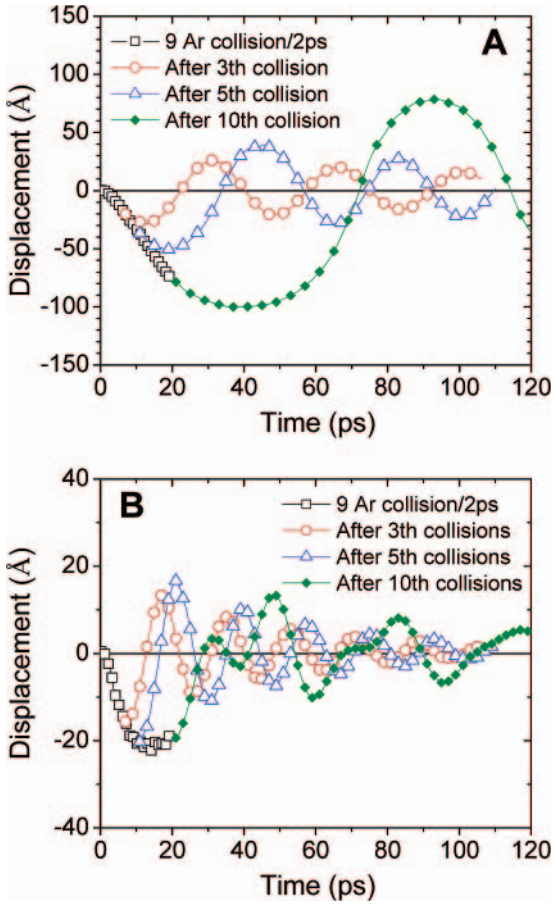

Figure 6. Displacements of (A) 165 Å-long, and (B) 115 Å-long (28,0) SWNTs responding to multiple collision events with Ar.

degree between 30 and 80 ps. Hence, the (16,16) SWNT recovers more slowly than the (28,0) SWNT.

More MD simulations have been done with shorter (165 and 115 Å) nanotubes (with 20 Å thermostat regions) to determine the effect of nanotube length on these results. In Figure 6 it is shown that the frequency of oscillation increases up to 50 GHz as the length of the SWNTs decreases. In other words, the amplitude of transverse vibration increases as the nanotube length increases. The simulations indicate that the damping of vibration depends on the nanotube length and

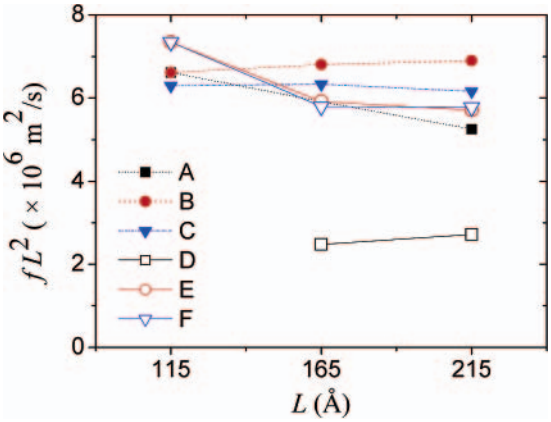

Figure 7. Plots of fL^2 vs L for (A) SWNT, (B) DWNT, and (C) TWNT following five collision events with Ar, (D) SWNT, (E) DWNT, (F) TWNT following ten collision events with Ar.

on the ratio of thermostat atoms to active atoms in the nanotube. This is caused by the fact that more thermostat atoms, which suppress their atomic motion to cool the system, more effectively decrease the kinetic energy of the shorter nanotube systems. The amplitudes of transverse vibration of 165 and 115 Å long-SWNTs decrease consecutively, as shown in Figure 6, while the damping of vibration of 215 Å-long SWNTs is hardly noticeable with much larger τ than that of shorter nanotubes, unless the nanotubes are buckled (see Figure 3 and Table 2). These same tendencies are found in simulations of (19,0)@(28,0) and (10,0)@(19,0)@(28,0) MWNTs of various lengths. The nanotube relaxation time τ decreases to 20 ps, and A_0 is reduced to as little as 5 Å, as the nanotube length decreases for SWNTs and MWNTs.

According to eq 2, fL^2 is independent of L if the diameters and number of nanotube walls are the same. Figure 6 shows that the DWNT (B) and the TWNT (C) follow the continuum-level formula over the whole L range after 5 Ar collision events, but the other nanotubes, which may be more easily buckled, hardly obey the formula, especially at short lengths.

In conclusion, the deflection of various nanotubes with a firmly fixed end in response to external impacts from incident Ar atoms is examined here with classical MD simulations. The dynamic behaviors of SWNTs, DWNTs, and TWNTs are compared. The deformation of the carbon nanotubes in the direction perpendicular to their axis is analyzed according to the relation between the amount of force imparted to the nanotubes and strain on the molecular bonds. The mechanical response and recovery of the nanotubes after release are compared for various nanotube configurations. The SWNTs, which are more flexible than the MWNTs, even buckle over during the relaxation stage that follows the collision events. As the number of collisions and the number of walls increase, the amplitude of nanotube oscillation increases. As the number of walls increases, the oscillations of the MWNTs are balanced in the upward and downward directions. The deflections of zigzag and armchair nanotubes have been compared for similar numbers of walls and nanotube diameters. As the nanotubes are shortened, the vibrational motion of the nanotubes is predicted to be damped by energy

dissipation. Understanding the mechanical response of carbon nanotubes to external atomic collisions is an important first step to understanding their response to external fluid flow, which is likely to influence the behavior of nanotube levers in applications such as NEMS. In addition, understanding the oscillatory deflection of nanotubes that have been displaced to a significant degree is also important in applications such as nanoactuators, nanoswitches, and nanotweezers, where large displacements are repeatedly induced.

Acknowledgment. K.-H.L. and S.B.S. gratefully acknowledge support from the Network for Computational Nanotechnology, funded through the National Science Foundation (EEC-0228390). P.K. was supported by the NSF Grant No. DMR 134725.

References

(1) Dequesnes, M.; Rotkin, S. V.; Aluru, N. R. *Nanotechnology* **2002**, *13*(1), 120−131.
(2) Kong, J.; Franklin, N. R.; Zhou, C.; Chapline, M. G.; Peng, S.; Cho, K.; Dai, H. *Science* **2000**, *287*, 622−625.
(3) Baughman, R. H.; Cui, C. X.; Zakhidov, A. A.; Iqbal, Z.; Barisci, J. N.; Spinks, G. M.; Wallace, G. G.; Mazzoldi, A.; De Rossi, D.; Rinzler, A. G.; Jaschinski, O.; Roth, S.; Kertesz, M. *Science* **1999**, *284*(5418), 1340−1344.
(4) Kim, P.; Lieber, C. M. *Science* **1999**, *286*(5447), 2148−2150.
(5) Shen, W.; Jiang, B.; Han, B. S.; Xie, S.-S. *Phys. Rev. Lett.* **2000**, *84*(16), 3634−3637.
(6) Li, F.; Cheng, H. M.; Bai, S.; Su, G.; Dresselhaus, M. S. *Appl. Phys. Lett.* **2000**, *77*(20), 3161−3163.
(7) Yu, M. F.; Lourie, O.; Dyer, M. J.; Moloni, K.; Kelly, T. F.; Ruoff, R. S. *Science* **2000**, *287*(5453), 637−640.
(8) Krishnan, A.; Dujardin, E.; Ebbesen, T. W.; Yianilos, P. N.; Treacy, M. M. J. *Phys. Rev. B* **1998**, *58*(20), 14013−14019.
(9) Wong, E. W.; Sheehan, P. E.; Lieber, C. M. *Science* **1997**, *277*(5334), 1971−1975.
(10) Qian, D.; Liu, W. K.; Ruoff, R. S. *Compos. Sci. Technol.* **2003**, *63*(11), 1561−1569.
(11) Robertson, D. H.; Brenner, D. W.; Mintmire, J. W. *Phys. Rev. B* **1992**, *45*(21), 12592−12595.
(12) Nardelli, M. B.; Yakobson, B. I.; Bernholc, J. *Phys. Rev. B* **1998**, *57*(8), R4277−R4280.
(13) Yakobson, B. I. *Appl. Phys. Lett.* **1998**, *72*(8), 918−920.
(14) Ni, B.; Sinnott, S. B.; Mikulski, P. T.; Harrison, J. A. *Phys. Rev. Lett.* **2002**, *88*(20), 205505 (1−4).
(15) Yakobson, B. I.; Brabec, C. J.; Bernholc, J. *Phys. Rev. Lett.* **1996**, *76*(14), 2511−2514.
(16) Srivastava, D.; Brenner, D. W.; Schall, J. D.; Ausman, K. D.; Yu, M. F.; Ruoff, R. S. *J. Phys. Chem. B* **1999**, *103*(21), 4330−4337.
(17) Popov, V. N.; Doren, V. E. V. *Phys. Rev. B* **2000**, *61*(4), 3078−3084.
(18) Srivastava, D.; Menon, M.; Cho, K. *Phys. Rev. Lett.* **1999**, *83*(15), 2973−2976.
(19) Marques, M. A. L.; Troiani, H. E.; Miki-Yoshida, M.; Jose-Yacaman, M.; Rubio, A. *Nano Lett.* **2004**, *4*(5), 811−815.
(20) Zhao, Y.; Ma, C. C.; Chen, G. H.; Jiang, Q. *Phys. Rev. Lett.* **2003**, *91*(17), 1705504-(1−4).
(21) Zheng, Q. S.; Jiang, Q. *Phys. Rev. Lett.* **2002**, *88*(4), 045503 1−3.
(22) Cumings, J.; Zettl, A. *Science* **2000**, *289*(5479), 602−604.
(23) Tuzun, R. E.; Noid, D. W.; Sumpter, B. G. *Nanotechnology* **1995**, *6*(2), 64−74.
(24) Yao, N.; Lordi, V. *J. Appl. Phys.* **1998**, *84*(15), 1939−1943.
(25) Raravikar, N. R.; Keblinski, P.; Rao, A. M.; Dresselhaus, M. S.; Schadler, L. S.; Ajayan, P. M. *Phys. Rev.* B **2002**, *66*(23), 235424.
(26) Brenner, D. W.; Shenderova, O. A.; Harrison, J. A.; Stuart, S. J.; Ni, B.; Sinnott, S. B. *J. Phys.: Condens. Matter* **2002**, *14*(4), 783−802.
(27) Charlier, A.; McRae, E.; Heyd, R.; Charlier, M. F.; Moretti, D. *Carbon* **1999**, *37*(11), 1779−1783.
(28) Ebbesen, T. W. *Phys. Today* **1996**, *49*(6), 26−32.
(29) Kiang, C. H.; Endo, M.; Ajayan, P. M.; Dresselhaus, G.; Dresselhaus, M. S. *Phys. Rev. Lett.* **1998**, *81*(9), 1869−1872.
(30) Dresselhaus, M.; Dresselhaus, G.; Avouris, Ph. *Carbon Nanotubes: Synthesis, Structure, Properties, and Applications*; Springer-Verlag: Berlin, 2001.
(31) Hernandez, E.; Goze, C.; Bernier, P.; Rubio, A. *Phys. Rev. Lett.* **1998**, *80*(20), 4502−4505.
(32) Zhang, P.; Lammert, P. E.; Crespi, V. H. *Phys. Rev. Lett.* **1998**, *81*(24), 5346−5349.

NL0481829